IOPscience iopscience.iop.org

Home Search Collections Journals About Contact us My IOPscience

Sources and implications of resonant mode splitting in silicon nanowire devices

This article has been downloaded from IOPscience. Please scroll down to see the full text article.

2011 Nanotechnology 22 455502

(http://iopscience.iop.org/0957-4484/22/45/455502)

View the table of contents for this issue, or go to the journal homepage for more

Download details:
IP Address: 128.46.220.170
The article was downloaded on 19/12/2011 at 15:13

Please note that terms and conditions apply.

Nanotechnology **22** (2011) 455502 (6pp) doi:10.1088/0957-4484/22/45/455502

Sources and implications of resonant mode splitting in silicon nanowire devices

M R Nelis[1,2], L Yu[1,3], W Zhang[4], Y Zhao[3], C Yang[1,3,4], A Raman[1,2], S Mohammadi[1,5] and J F Rhoads[1,2,6]

[1] Birck Nanotechnology Center, Purdue University, West Lafayette, IN 47907, USA
[2] School of Mechanical Engineering, Purdue University, West Lafayette, IN 47907, USA
[3] Department of Physics, Purdue University, West Lafayette, IN 47907, USA
[4] Department of Chemistry, Purdue University, West Lafayette, IN 47907, USA
[5] School of Electrical Engineering, Purdue University, West Lafayette, IN 47907, USA
[6] Ray W Herrick Laboratories, Purdue University, West Lafayette, IN 47907, USA

E-mail: jfrhoads@purdue.edu

Received 22 June 2011, in final form 23 June 2011
Published 21 October 2011
Online at stacks.iop.org/Nano/22/455502

Abstract
This work investigates the effects of asymmetric cross-sectional geometry on the resonant response of silicon nanowires. The work demonstrates that dimensional variances of less than 2% qualitatively alter a nanosystem's near-resonant response, yielding a non-Lorentzian frequency response structure, which is a direct consequence of resonant mode splitting. Experimental results show that this effect is independent of device boundary conditions, and can be easily modeled using continuous beam theory. Proper understanding of this phenomenon is believed to be essential in the characterization of the dynamic response of resonant nanowire systems, and thus the predictive design of such devices.

(Some figures in this article are in colour only in the electronic version)

1. Introduction

Resonant nanowire systems have demonstrated utility in applications ranging from radio frequency (RF) filtering and mass sensing to quantum-level detection [1, 2]. The functionality of these devices is commonly founded upon the single-peak, Lorentzian frequency response structure that is associated with a predominately single-degree-of-freedom resonator. Nanofabrication process variability results in structures with asymmetric cross-sectional geometries. Silicon nanowires, for example, commonly feature irregular hexagonal cross sections [3, 4], as shown in figure 1. Small dimensional variances and asymmetries (often <2% of the nominal dimension) qualitatively alter a nanosystem's near-resonant response, yielding a multi-peak, non-Lorentzian frequency response structure (provided that the ambient pressure is sufficiently low enough that the peaks do not overlap—see figure 2). This mode splitting effect has been experimentally verified by Biedermann, Gil-Santos, and their respective collaborators [5, 6]. Given the endemic nature of this response feature in all resonant nanowire devices, particular care must be taken to account for this effect in the course of predictive device design.

2. Modeling

Generally speaking, resonant mode splitting does not occur in devices with circular or regular hexagonal cross sections, as the orthogonal modes of vibration, transverse to the cross-sectional plane, associated with each resonance occur at identical frequencies in these systems. In the presence of cross-sectional irregularity, each of these resonance peaks split, yielding nearly orthogonal modes with distinct natural frequencies. This effect also occurs in elliptical cross sections, as observed by Garrett [7].

By using a model that parameterizes an irregular hexagon by the largest vertex-to-vertex distance (a) and perpendicular width (b), see figure 1, the frequencies of a given nanowire's split modes can be represented by a continuous beam in lateral vibration with undamped natural frequencies (in Hz) given by $f_{a,b}$, where

$$f_{a,b} = \frac{\beta^2}{2\pi}\sqrt{\frac{EI_{a,b}}{\rho A}}. \quad (1)$$

Here, β is a boundary condition dependent modal factor, EI represents the system's flexural rigidity, ρ represents

 © 2011 IOP Publishing Ltd Printed in the UK & the USA

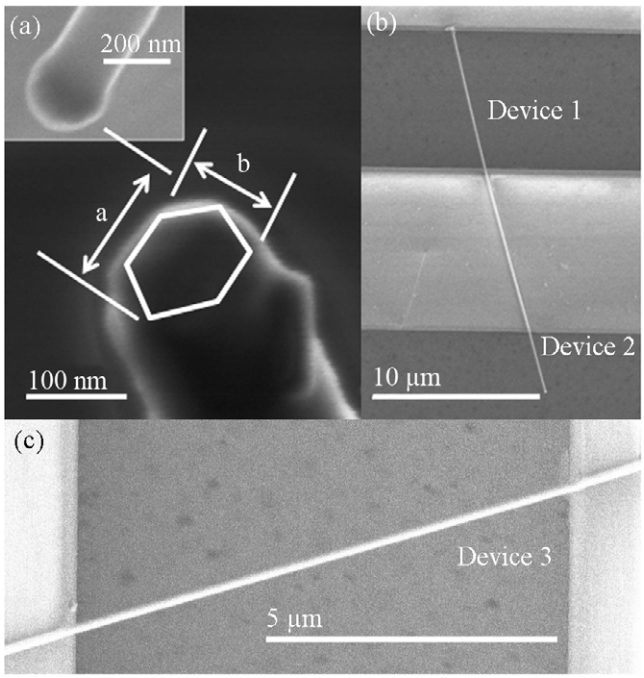

Figure 1. (a) Scanning electron micrograph (SEM) of a silicon nanowire's cross section. Note that the inset highlights the catalyst remaining on the end of an intact wire following fabrication. (b) SEM of two typical devices. Note that the lighter regions here are the SU-8 grating, while the darker regions are the silicon substrate. Device 1 features an effective fixed-pinned boundary condition, while device 2 is cantilevered. (c) SEM of device 3, a silicon nanowire with fixed–fixed boundary conditions.

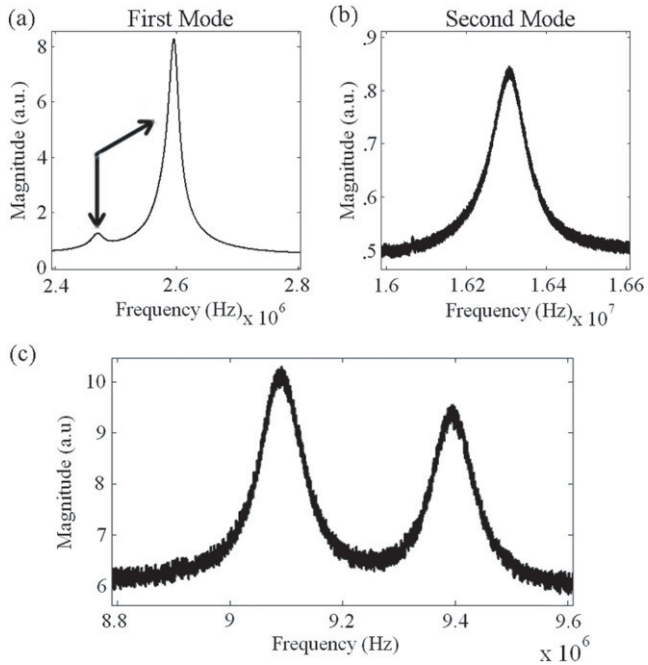

Figure 2. The experimental frequency response of silicon nanowires excited by thermal noise, as measured at room temperature in a 2 mTorr environment. Insets (a) and (b) highlight the response of a cantilevered nanowire near its first and second modes of vibration. Note that inset (a) shows resonant mode splitting, while inset (b) does not. The absence of resonant mode splitting near the second mode of oscillation may be due to the resonant response being below the thermomechanical noise floor. Inset (c) highlights the response of a fixed–fixed nanowire near its first mode of vibration. Appreciable mode splitting is evident.

the system's mass density, A defines the resonator's cross-sectional area, and I_a and I_b delineate the device's cross-sectional moments of inertia. The latter parameters are defined according to:

$$A = \frac{3ab}{4}, \tag{2}$$

$$I_a = \frac{5a^3b}{128}, \tag{3}$$

$$I_b = \frac{5ab^3}{96}. \tag{4}$$

Note that when a and b are parameterized such that the hexagon is regular, the values of I_a and I_b are identical.

The aforementioned split in resonant frequencies and associated modes can be quantified by defining a mistuning metric as the ratio between the difference in the split frequencies and the center frequency. As verified by substituting equation (1) into (5), the mistuning metric δ is only a function of the vertex-to-vertex distance (a) and the perpendicular width (b)

$$\delta = \frac{2(f_a - f_b)}{f_a + f_b} = \frac{2\sqrt{3}a - 4b}{\sqrt{3}a + 2b}. \tag{5}$$

This means that regardless of boundary conditions and material properties, the mistuning exhibited by a nanowire system is only a function of the geometry of the cross section.

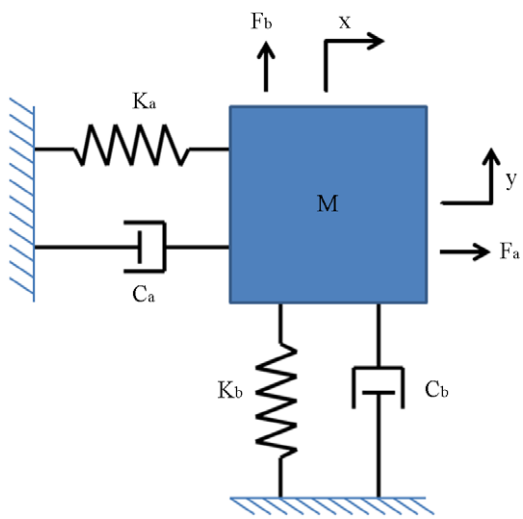

Figure 3. A schematic of the two-degree-of-freedom model for a mistuned resonator.

Accordingly, the only way to avoid mistuning in such systems is to have a perfectly regular cross section.

For analytical purposes, the nanowire can also be modeled in an approximate sense as a two-degree-of-freedom uncoupled system, as shown in figure 3. Note that the damping coefficients, C_a and C_b, and the applied forces, F_a and

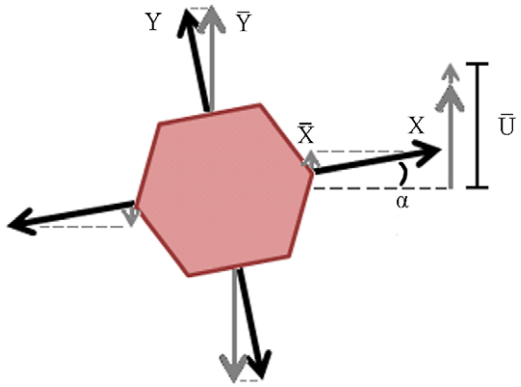

Figure 4. A schematic of the effect of viewing angle on the measured magnitude of displacement for the two modes.

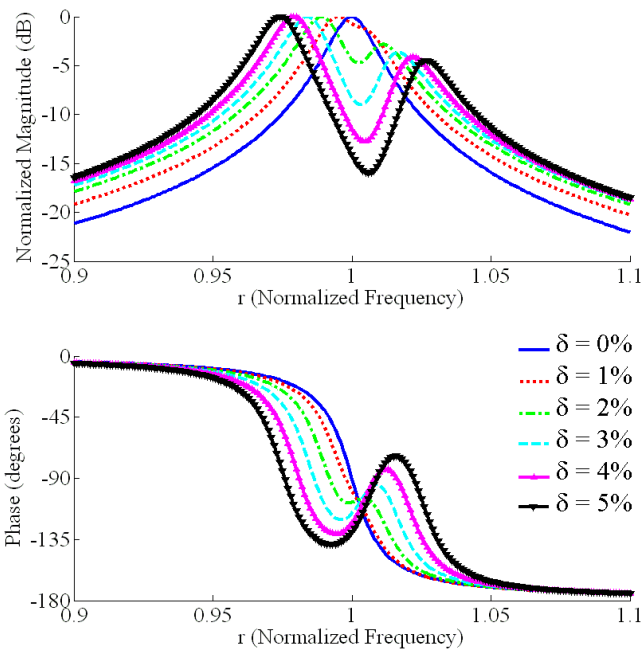

Figure 5. Theoretical frequency response of the silicon nanowire as a function of mistuning. Assumed system properties: $Q = 60$, $\alpha = \frac{\pi}{6}$ rad.

F_b, included here are assumed to be equal, and the spring constants, K_a and K_b distinct. This results in a relationship between the natural frequencies and quality factors given by:

$$\frac{\omega_a}{Q_a} = \frac{\omega_b}{Q_b} = \frac{\omega_n}{Q}. \tag{6}$$

Using these relationships as a functional basis, nominal quality factors and natural frequencies for the system can be defined according to:

$$Q = \frac{Q_a}{1+\delta/2} = \frac{Q_b}{1-\delta/2} \tag{7}$$

$$\omega_n = \frac{\omega_a}{1+\delta/2} = \frac{\omega_b}{1-\delta/2} = \frac{\omega_a+\omega_b}{2}. \tag{8}$$

When the excitation frequency is non-dimensionalized with respect to ω_n, and the two equations of motion are

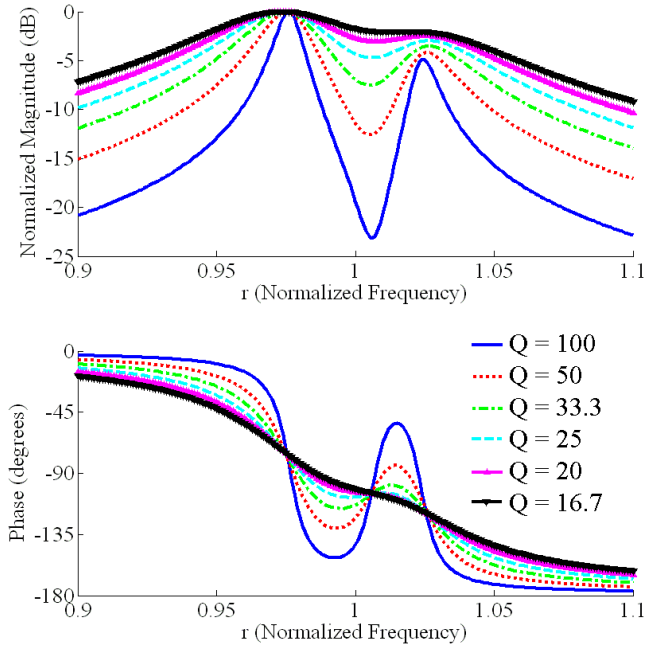

Figure 6. Theoretical frequency response of the silicon nanowire as a function of quality factor. Assumed system properties: $\delta = 4.73\%$, $\alpha = \frac{\pi}{6}$ rad.

simplified, (9) and (10) result:

$$Z_a = \frac{X}{\hat{F}_a} = \frac{1}{\omega_n^2(-r^2 + \imath r/Q + (1+\delta/2)^2)} \tag{9}$$

$$Z_b = \frac{Y}{\hat{F}_b} = \frac{1}{\omega_n^2(-r^2 + \imath r/Q + (1-\delta/2)^2)} \tag{10}$$

$$r = \frac{\sigma}{\omega_n}. \tag{11}$$

In the equations above σ and r are the excitation frequency and normalized excitation frequency, respectively, and $\hat{F}_a$ and $\hat{F}_b$ are the mass normalized applied forces. Note that both equations of motion are identical if there is no mistuning. In practice, when the system displacement is measured, only the out-of-plane motion can be resolved, so a new variable α is introduced which captures the projection effect due to viewing angle and orientation, as shown in figure 4. This renders an observable net displacement given by:

$$\overline{U} = |X \sin\alpha + Y \cos\alpha|. \tag{12}$$

Analysis of this simple model reveals the experimentally observable effects associated with variations of Q, δ, and α, as succinctly highlighted in figures 5–7. Of particular note in these figures is the non-Lorentzian nature of the system's response and the fact that the observable quality factor is distorted by the relative proximity of the modes (see figure 6). This appears to indicate that conventional Q approximation techniques are insufficient for use with resonant nanosystems with some degree of mode splitting. Also of note is the fact that wire orientation has a dramatic effect on both the quantitative and qualitative nature of the observable response (see figure 7).

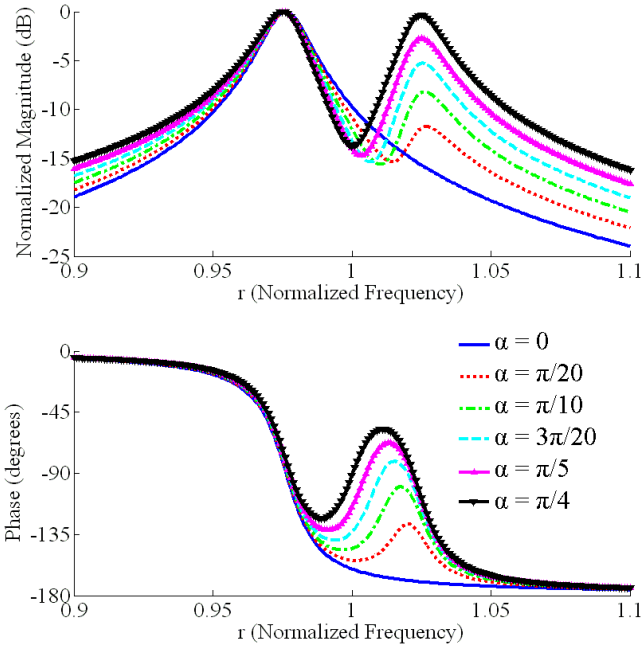

Figure 7. Theoretical frequency response of the silicon nanowire as a function of viewing angle. Assumed system properties: $Q = 60$, $\delta = 4.73\%$.

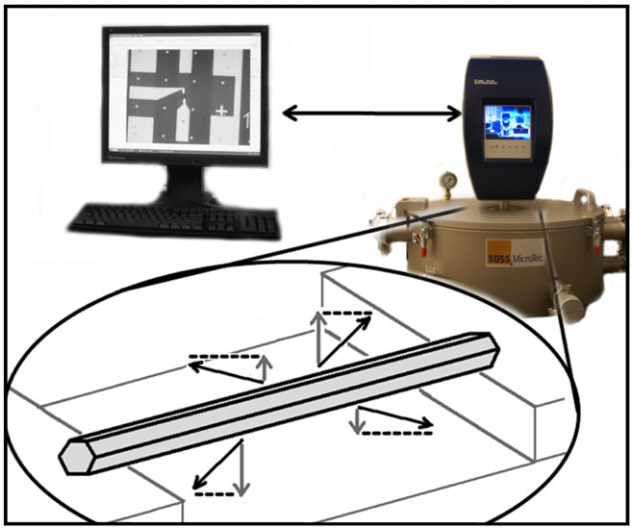

Figure 8. A schematic of the experimental setup, consisting of a computer-based data acquisition/processing station, Polytec MSA-400 scanning laser Doppler vibrometer, and a Suss Microtec PLV-50 optically accessible vacuum chamber. Note that the measured displacement is a projection of the device's actual displacement, measured normal to the substrate and is only proportional to the physical response, since the laser's spot size is approximately ten times larger than the nanowires' diameter. In the inset, the black arrows indicate the actual motion of the wire, and the dark gray arrows indicate the measured displacement.

3. Device fabrication

Silicon nanowires (150 nm in nominal width) were synthesized using the nanocluster-catalyzed vapor–liquid–solid method. In this process, growth is realized through the use of 150 nm gold nanocluster catalysts in conjunction with a silicon reactant (silane), P-type dopant (diborane gas balanced with hydrogen gas), and hydrogen carrier. Following synthesis, the wires were removed from the growth substrate via sonication and dissolved into isopropyl alcohol. The wires were then deposited by dropper (randomly dispersed) onto a silicon substrate with a 10 μm SU-8 grating pattern. Near field forces were exploited for anchoring. Figure 1 shows a typical nanowire device. Note that since the silicon nanowires examined herein derive from a single fabrication batch, they feature nominally identical material properties. Accordingly, device to device variations in frequency arise solely from varying boundary conditions and length, as well as cross-sectional irregularity.

4. Experiment

Following fabrication, a scanning laser Doppler vibrometer was used to measure the thermally excited displacement response of the nanowire devices in the direction perpendicular to the device substrate, as shown in figures 8 and 4. The adopted measurement procedure mirrors that previously used by Biedermann *et al* [5, 8] and is akin to that utilized by Belov *et al* [9]. Samples were measured at room temperature in a 2 mTorr environment. This setting ensured that surface effects and anchor losses were the primary source of dissipation ($Q = 30$–200) and not molecular-regime fluid damping. Note that the utilized vibrometer could only resolve out-of-plane motions of the thermally excited system with an effective displacement noise floor of approximately 150 fm. In addition, the planes of vibrations were oriented at an unknown angle with respect to the substrate due to the random dispersion of the nanowires (as is commonly the case in final device implementations). As a result, the split modes featured orientation-dependent resonant amplitudes, as highlighted in figures 2 and 7.

5. Results

Theory predicts that mode splitting occurs as a function of cross section geometry. Experimental data appear to validate this, in that resonant mode splitting occurred in most of the examined nanowires, regardless of the length of, or boundary conditions associated with, the device (see table 1). Note that the measured frequencies are all within the geometry-based uncertainty of the theoretical predictions and match within 5%.

The actual mistuning between the modes was extrapolated by substituting the peak frequencies into (5). The mistuning values that could be calculated from the experimental data ranged from 2% to 10%. A mistuning value of 3% was the most common value of the 13 devices that showed mode splitting. For the cases where no mode splitting was observed either the mistuning was smaller than 2%, resulting in obscured peaks, or the viewing angle was such that contributions from the other mode were minimal.

Small magnitudes, the thermomechanical/measurement noise floor, and the lack of phase information all contributed to

Table 1. Theoretical and experimental natural frequencies of the silicon nanowires. Assumed material and geometric properties: $\rho = 2339$ kg m^{-3}, $E = 189$ GPa, $a = 159$ nm, and $b = 148$ nm. Quality factors were large enough to allow direct comparison between undamped theory and the experiment for the displayed significant figures. Also note that C = cantilevered; FP = fixed-pinned; and FF = fixed-fixed boundary conditions. Finally, stars in the mistuning column indicate systems where splitting was present but the second frequency could not be recovered.

Boundary condition	Length (μm)	Undamped theory (MHz)		Experiment (MHz)		Mistuning (%)
C1 mode 1	8.42	2.61 ± 0.17	2.74 ± 0.19	2.47	2.6	4.934
C1 mode 2	8.42	16.36 ± 1.09	17.16 ± 1.17	16.31	—	—
C2	6.92	3.87 ± 0.30	4.05 ± 0.32	—	3.98	—
C3	7.39	3.39 ± 0.25	3.55 ± 0.27	3.11	—	*
C4	6.81	3.99 ± 0.32	4.18 ± 0.34	3.77	3.90	3.372
C5	5.66	5.78 ± 0.54	6.06 ± 0.58	5.68	5.82	2.435
C6	5.43	6.28 ± 0.61	6.58 ± 0.63	6.15	6.34	3.004
C7	4.93	7.62 ± 0.81	7.99 ± 0.83	6.84	7.32	6.853
FP1	8.92	10.12 ± 0.65	10.69 ± 0.70	—	10.61	—
FP2	9.59	8.82 ± 0.53	9.25 ± 0.57	8.46	9.14	7.765
FP3	9.21	9.57 ± 0.60	10.03 ± 0.64	—	10.56	—
FP4	9.76	8.52 ± 0.51	8.93 ± 0.55	8.27	9.14	9.960
FF1	11.33	8.95 ± 0.48	9.62 ± 0.53	9.09	9.39	3.215
FF2	10.40	10.89 ± 0.62	11.42 ± 0.67	10.47	10.80	3.103
FF3	9.41	13.30 ± 0.82	13.95 ± 0.88	14.60	15.11	3.456
FF4	10.55	10.58 ± 0.60	11.10 ± 0.65	—	12.15	—
FF5	13.07	6.90 ± 0.34	7.23 ± 0.37	6.79	7.17	5.305
FF6	9.73	12.44 ± 0.74	13.05 ± 0.80	12.50	—	—
FF7	9.76	12.37 ± 0.74	12.97 ± 0.80	11.86	—	—
FF8	10.05	11.66 ± 0.68	12.23 ± 0.73	—	12.85	—
FF9	10.24	11.23 ± 0.65	11.78 ± 0.70	—	12.08	—
FF10	9.12	14.16 ± 0.89	14.85 ± 0.96	14.46	14.68	1.556
FF11	10.33	11.04 ± 0.63	11.57 ± 0.68	—	12.10	*
FF12	10.35	11.00 ± 0.63	11.53 ± 0.68	—	11.80	—

the difficulty in matching the analytically predicted frequency response with experimental results. Despite these issues, in some instances it was possible to use nonlinear regression to fit the model presented herein to the experiments. Figure 9 shows the model presented in (12) plotted with experimental data recovered from a cantilevered nanowire. As evident, there is appreciable fidelity between the simple model and experiment.

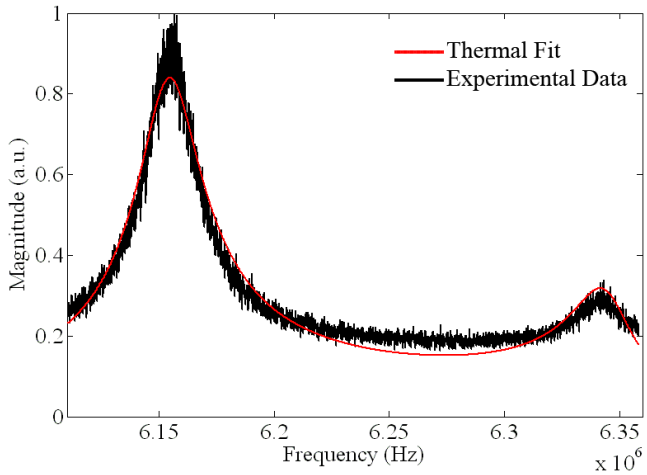

Figure 9. The frequency response of cantilevered device 8 from table 1 fitted with the model presented in (12). The experimentally recovered and regression validated center frequency is approximately 6.249 MHz, and the mistuning 3.04%.

6. Conclusion

Mode splitting in silicon nanowire systems occurs due to geometry-based irregularities in their cross sections. This effect is independent of material properties and boundary conditions of the devices, and occurs even when the dimensional differences between them are on the order of 2% of their nominal values. In this paper the mode splitting was modeled by parameterizing a hexagon, and using a simple two-degree-of-freedom mechanical model to qualitatively and quantitatively capture pertinent dynamics. This modeling approach accurately reflected experimental data in nanowire systems where mode splitting was evident.

Given the simplicity of the systems examined herein, non-Lorentzian frequency responses, akin to those presented here, can be expected in most nanowire devices. Accordingly, designers of functional nanoscale devices, such as resonant mass sensors and electromechanical signal processing elements, should account for this mechanism in the course of device design. For example, in resonant mass sensing applications, device designers should not only account for added mass and stiffness change effects, but also for quantitative changes in coupling between the split resonant modes. This added complexity should not be seen as a technical deterrent, but rather as an opportunity for innovative devices and resonant tuning, as the intentional varying of process parameters should lead to a direct alteration of a given resonator's near-resonant response. Ongoing efforts are aimed at exploiting this opportunity and investigating the effects of cross-sectional asymmetry in the presence of noise, nonlinearity, and/or parametric effects.

Acknowledgment

This work was supported by the National Science Foundation under grant 0826276.

References

[1] Guerra D N, Dunn T and Mohanty P 2009 *Nano Lett.* **9** 3096
[2] Naik A K, Hanay M S, Hiebert W K, Feng X L and Roukes M L 2009 *Nature Nanotechnol.* **4** 445
[3] Feng X L, He R, Yang P and Roukes M L 2007 *Nano Lett.* **7** 1953
[4] Tian B, Zheng X, Kempa T J, Fang Y, Yu N, Yu G, Huang J and Lieber C M 2007 *Nature* **449** 885
[5] Biedermann L B, Tung R C, Raman A, Reifenberger R G, Yazdanpanah M M and Cohn R W 2010 *Nanotechnology* **21** 305701
[6] Gil-Santos E, Ramos D, Martìnez J, Fernàndex-Regùlez M, Garcìa R, San Paulo À, Calleja M and Tamayo J 2010 *Nature Nanotechnol.* **5** 641–5
[7] Garrett S L 1990 *J. Acoust. Soc. Am.* **88** 210
[8] Biedermann L B, Tung R C, Raman A and Reifenberger R G 2009 *Nanotechnology* **20** 035702
[9] Belov M, Quitoriano N J, Sharma S, Hiebert W K, Kamins T I and Evoy S 2008 *J. Appl. Phys.* **103** 074304